Reaction energetics and crystal structure of $Li_4BN_3H_{10}$ from first principles

Donald J. Siegel and C. Wolverton
Physical and Environmental Sciences Department, Ford Motor Company, MD3083/RIC, Dearborn, Michigan 48121, USA

V. Ozoliņš
Department of Materials Science and Engineering, University of California, Los Angeles, California 90095, USA
(Received 25 July 2006; published 2 January 2007)

Using density functional theory we examine the crystal structure and the finite-temperature thermodynamics of formation and dehydrogenation for the quaternary hydride $Li_4BN_3H_{10}$. Two recent studies based on x-ray and neutron diffraction have reported three bcc crystal structures for this phase. While these structures possess identical space groups and similar lattice constants, internal coordinate differences result in bond length discrepancies as large as 0.2 Å. Geometry optimization calculations on the experimental structures reveal that the apparent discrepancies are an artifact of x-ray interactions with strong bond polarization; the relaxed structures are essentially identical. Regarding reaction energetics, the present calculations predict that the formation reaction $3LiNH_2+LiBH_4 \rightarrow Li_4BN_3H_{10}$ is exothermic with enthalpy $\Delta H^{T=300\ K}=-11.8$ kJ/(mol f.u.), consistent with reports of spontaneous $Li_4BN_3H_{10}$ formation in the literature. Calorimetry experiments have been reported for the dehydrogenation reaction, but have proven difficult to interpret. To help clarify the thermodynamics we evaluate the free energies of seventeen candidate dehydrogenation pathways over the temperature range $T=0-1000$ K. At temperatures where H_2 release has been experimentally observed ($T\approx 520-630$ K), the favored dehydrogenation reaction is $Li_4BN_3H_{10} \rightarrow Li_3BN_2+LiNH_2+4H_2$, which is weakly endothermic [$\Delta H^{T=550\ K}=12.8$ kJ/(mol H_2)]. The small calculated ΔH is consistent with the unsuccessful attempts at rehydriding reported in the literature, and suggests that the moderately high temperatures needed for H desorption result from slow kinetics.

DOI: 10.1103/PhysRevB.75.014101 PACS number(s): 64.70.Hz, 65.40.−b, 71.15.Nc, 81.05.Zx

I. INTRODUCTION

Recent efforts to improve the efficiency and reduce the environmental impact of automobile transport have focused on hydrogen-based fuel cells (FCs) and internal combustion engines (H_2ICEs) as possible replacements for current technologies powered by fossil fuels.[1] A significant obstacle to realizing this transition is the on-board storage of hydrogen at high gravimetric and volumetric densities.[2] To achieve the storage densities necessary for mobile applications, novel means for H storage are necessary, and a set of targets has been established to guide the search for new storage systems.[3] At present no known storage material or mechanism meets these targets.

One promising avenue for efficient storage of hydrogen is via solid state storage, such as in the form of complex or metal hydrides. Solid storage has the advantage of providing volumetric densities beyond what can be achieved with compressed H_2 gas or cryogenic liquid storage. However, all known hydrides suffer from one or more of the following limitations: low gravimetric densities, high H-desorption temperatures, or an inability to be easily rehydrided. The search for new hydrides that overcome these limitations has attracted intense interest during the past five years.

Toward these ends, recent experiments by Pinkerton and co-workers[4–6] and Aoki *et al.*[7,8] on the H-storage properties of the quaternary Li-B-N-H system are noteworthy. By mixing lithium borohydride ($LiBH_4$) and lithium amide ($LiNH_2$), both groups have reported the formation of a hydride phase that when heated above ~520 K released approximately 10 wt % hydrogen. While the reported desorption temperature is somewhat too high, and reversibility has not yet been demonstrated, improvement in these areas may be possible (and has been partially demonstrated[6]) through the addition of catalytic dopants[6,9] or via novel synthetic routes,[10] suggesting that further study of this system is warranted.

The composition of the new Li-B-N-H phase was preliminarily identified[4] as "$Li_3BN_2H_8$," but subsequent experiments based on single-crystal x-ray diffraction[11] and synchrotron x-ray and neutron powder diffraction,[12] identified its true stoichiometry as $Li_4BN_3H_{10}$. Combined, these diffraction experiments identified three similar crystal structures, all sharing the bcc space group $I2_13$ with lattice constant $a=10.66-10.68$ Å, but with somewhat different internal coordinates. The discrepancy in atomic positions results in N-H bond lengths that differ between structures by as much as 0.2 Å, with smaller N-H lengths reported for the x-ray structures. It has been suggested that the discrepancy may be an artifact of x-ray interactions with strongly polarized electron clouds along the N-H bond direction.[11]

A careful characterization of a hydride's crystal structure is desirable because it enables an independent, *ab initio* assessment of the thermodynamics of hydrogen desorption and absorption reactions. Such an assessment is of value because it can clarify the thermodynamics when calorimetry measurements yield ambiguous results, such as in situations where multiple reactions occur simultaneously (see below). A key thermodynamic property which determines the suitability of a hydride for H-storage applications, is the strength of the hydrogen-host bond. The bond strength is quantified via the change in enthalpy (ΔH) occurring during hydrogen uptake and release. In mobile FC applications, for example,

it is desirable that the desorption reaction be *endothermic* ($\Delta H > 0$) with $\Delta H \approx 20-50$ kJ/(mol H_2). Neglecting kinetics, an enthalpy in this range would allow for H desorption at temperatures compatible with the waste heat from a FC, and permit on-board recharging under reasonable H_2 pressure.

Unfortunately, calorimetric measurements of H desorption in $Li_4BN_3H_{10}$ have been difficult to interpret. (See Refs. 6 and 8, and the supplementary information accompanying Ref. 4.) Because $Li_4BN_3H_{10}$ melts at ~460 K, approximately 60 K below the onset of H desorption, hydrogen gas evolves from the liquid state.[4] Concurrent with H_2 release is the formation of a solid reaction product, generally involving one or more polymorphs of Li_3BN_2 along with other unidentified phases,[4,7,8] and desorption of 2–3 mol % ammonia.[4] Measurements based on differential scanning calorimetry[4,6] (DSC) and differential thermal analysis[8] (DTA) suggest that the net heat flow during dehydriding is exothermic ($\Delta H < 0$). However, it is unclear what fraction of the total thermal profile arises from the exothermic latent heat of Li_3BN_2 solidification,[8] and furthermore how H_2 and NH_3 release impacts the calorimeter response.[4] Consequently, it has not been possible to unambiguously assess the endo- or exothermic nature of H desorption alone. Neglecting kinetic effects, the fact that it has proven very difficult[4] to rehydride $Li_4BN_3H_{10}$ suggests that desorption is weakly endothermic or exothermic. Regarding $Li_4BN_3H_{10}$ formation, several studies[4,8,12] have reported the spontaneous formation of $Li_4BN_3H_{10}$ after mixing $LiBH_4$ with $LiNH_2$, even at temperatures as low as room temperature, suggesting that the formation reaction is exothermic.[4]

In light of the discrepancy noted above regarding the crystal structure of $Li_4BN_3H_{10}$, and the additional ambiguity surrounding its dehydrogenation thermodynamics, we employ density functional theory[13,14] (DFT) calculations in an attempt to clarify these issues. First, we determine the ground state crystal structure by performing separate geometry optimization calculations on each of the experimentally proposed crystal structures. We find that the relaxed structures are essentially identical, and have N-H bond lengths that are consistent with the structure based on neutron diffraction,[12] thus confirming the conjecture[11] that the anomalously short N-H bond lengths observed in Ref. 11 are an artifact of x-ray measurements. Second, we evaluate the finite-temperature reaction enthalpies and free energies for the formation and dehydrogenation of $Li_4BN_3H_{10}$. $Li_4BN_3H_{10}$ formation (with respect to $LiNH_2$ and $LiBH_4$) is found to be exothermic, in agreement with experimental reports of spontaneous $Li_4BN_3H_{10}$ formation in the literature.[4,7,12] For H_2 desorption we explore the thermodynamics of 17 candidate reactions over the temperature range $T=0-1000$ K, as there appears to be some uncertainty in determining the reaction products experimentally.[4,7] At temperatures where desorption has been reported[4] ($T \approx 520-630$ K), the favored reaction is predicted to be $Li_4BN_3H_{10} \rightarrow Li_3BN_2 + LiNH_2 + 4H_2$, which is weakly endothermic. Moreover, the calculated free energies suggest that $Li_4BN_3H_{10}$ is a metastable phase that should decompose via one of three temperature-dependent pathways.

II. METHODOLOGY

First-principles calculations were performed using a plane-wave method based on the Perdew-Wang 1991 (PW91) generalized gradient approximation[15] to density functional theory[13,14] (VASP).[16] The core-valence electron interaction was treated using Blöchl's projector augmented wave (PAW) method,[17,18] and k-point sampling was performed on a dense Monkhorst-Pack[19] grid with an energy convergence of better than 1 meV per supercell. (In the case of $Li_4BN_3H_{10}$, a $2\times2\times2$ grid was sufficient to acheive this level of precision.) Electronic occupancies were determined via a Gaussian smearing algorithm with a 0.1 eV smearing width. For high-precision calculation of static 0 K (omitting zero-point vibrational effects) electronic energies and crystal structures we used the so-called hard VASP PAW potentials[20] with a plane-wave cutoff of 875 eV, and a geometry relaxation tolerance of better than 0.02 eV/Å. Internal atomic positions and external cell shape and volume were optimized simultaneously.

Finite-temperature thermodynamics were evaluated within the harmonic approximation.[21,22] Vibrational frequencies (ω_i) were extracted by diagonalizing a dynamical matrix whose elements were determined via the so-called direct method:[23] the forces generated by series of symmetry inequivalent atomic displacements about the equilibrium geometry (±0.02 Å, ±0.04 Å) were fitted to cubic splines in order to extract the force constants. Because large supercells are desirable to minimize finite-size effects, and with the exception of the molecular species (H_2, N_2, NH_3) where the number of atoms per supercell is small, the dynamical matrix calculations on the solid-state phases were preformed using a softer set of PAW potentials[24] and plane-wave cutoff energies ranging from 400 to 500 eV.[25] A comparison of calculated structural parameters and formation energies with existing experimental and theoretical data is presented in the following section.

Once the normal-mode frequencies have been determined, finite-temperature energetics can be obtained by enthalpic (H_{vib}) and entropic (S_{vib}) additions to the static electronic energies. Within the harmonic approximation these contributions are given by[21]

$$H_{\text{vib}}(T) = \sum_i \frac{1}{2}\hbar\omega_i + \hbar\omega_i \left[\exp\left(\frac{\hbar\omega_i}{k_B T}\right) - 1 \right]^{-1}, \qquad (1)$$

$$S_{\text{vib}}(T) = k_B \sum_i \frac{\hbar\omega_i / k_B T}{\exp(\hbar\omega_i / k_B T) - 1} - \ln\left[1 - \exp\left(\frac{-\hbar\omega_i}{k_B T}\right) \right], \qquad (2)$$

where the sums run over vibrational frequencies ($3N-3$ frequencies for solids and nonlinear molecules, $3N-5$ frequencies for linear molecules), k_B is the Boltzmann factor, and T is the absolute temperature. For the linear (nonlinear) molecules an additional $\frac{7}{2}k_B T$ ($4k_B T$) term is added to Eq. (1) to account for translational, rotational, and pV degrees of freedom. The zero-point energy (ZPE) can be recovered from Eq. (1) in the limit $H_{\text{vib}}(T=0)$. The enthalpy and free energy of a phase can therefore be expressed as

$$H(T) = E + H_{\mathrm{vib}}(T), \tag{3}$$

$$G(T) = H(T) - S(T)T, \tag{4}$$

where E is the static electronic energy of the crystal/molecule in its ground-state geometry and S represents either the standard tabulated[28] entropy of a given molecular species in the gas phase at $p=1$ bar [$S_0^{T=300\ \mathrm{K}}=130.858$ (H_2), 191.789 (N_2), and 192.995 J K^{-1} mol^{-1} (NH_3)], or the vibrational entropy S_{vib} of a solid-state phase.

III. CRYSTAL STRUCTURE

The crystal structure of $Li_4BN_3H_{10}$ has been studied by two groups.[11,12] Filinchuk and co-workers[11] used single-crystal x-ray diffraction to identify the structures of the two largest crystal domains obtained after remelting a 2:1 mixture of $LiNH_2$ and $LiBH_4$. Both domains exhibited a bcc structure (space group $I2_13$) with lattice constants of 10.67–10.68 Å. Chater *et al.*[12] used a combination of high-resolution synchrotron x-ray and neutron diffraction to examine powder samples prepared from a wide range of $LiNH_2$:$LiBH_4$ compositions. They determined that although the most likely stoichiometric composition was 3:1, the $Li_4BN_3H_{10}$ structure was able to accommodate a wide range of stoichiometries. Their best-fit crystal structure had external cell parameters similar to those reported in Ref. 11: bcc (space group $I2_13$) with $a=10.66$ Å. Despite the good agreement in external geometries, the structures obtained by these two studies differ markedly in their internal coordinates. Most notably, the single-crystal x-ray diffraction

TABLE I. Calculated structural parameters compared with experimental data. Bond lengths (d) and crystal lattice constants (a, b, c) are given in Å, bond angles ($\measuredangle$) and angles between lattice vectors (α, β) are listed in degrees. Space group information for the solid phases is listed in parentheses.

System	Parameter	Calculated	Experiment	Reference
H_2	d(H-H)	0.749	0.741	27
N_2	d(N-N)	1.101	1.098	27
NH_3	d(N-H)	1.021	1.012	27
	$\measuredangle$(H-N-H)	106.4	106.7	27
α-B ($R\bar{3}m$)	a	5.05	5.06	29
	α	58.1	58.1	29
BN ($F\bar{4}3m$)	a	3.62	3.62	30
Li ($Im\bar{3}m$)	a	3.44	3.51	31
LiH ($Fm\bar{3}m$)	a	4.01	4.07	32
Li_3N ($P\bar{3}m1$)	a	3.64	3.61[a]	
	c	3.88	3.85[a]	
$LiNH_2$ ($I\bar{4}$)	a	5.02	5.04	34
	c	10.28	10.28	34
Li_2NH ($Pnma$)	a	7.75	7.73[b]	
	b	3.61	3.60[b]	
	c	4.88	4.87[b]	
α-Li_3BN_2 ($P4_2/mnm$)	a	4.67	4.64	36 and 37
	c	5.22	5.26	36 and 37
β-Li_3BN_2 ($P2_1/c$)	a	5.15	5.15	38
	b	7.08	7.08	38
	c	6.77	6.79	38
	β	112.7	113.0	38
Li_3BN_2 ($I4_1/amd$)	a	6.63	6.60	39
	c	10.35	10.35	39
$LiBH_4$ ($Pnma$)	a	7.25	7.18	40
	b	4.38	4.44	40
	c	6.63	6.80	40
$Li_4BN_3H_{10}$ ($I2_13$)	a	10.60	10.67–10.68	11
			10.66	12

[a]Theoretically predicted structure from Ref. 33. In agreement with Ref. 33, we find the room-temperature experimental $P6/mmm$ structure to be unstable at low temperature, with a weak soft mode of $66i$ cm^{-1}.
[b]Theoretically predicted structure from Ref. 35.

TABLE II. Calculated relaxed internal atomic positions of $Li_4BN_3H_{10}$ compared with experimental measurements from Refs. 11 and 12.

	Calculated			Experiment		
Atom	x	y	z	x	y	z
			Domain 1, Ref. 11			
N	0.117	0.362	0.402	0.115	0.359	0.405
B	0.113	0.113	0.113	0.114	0.114	0.114
Li1	0.281	0.000	0.250	0.287	0.000	0.250
Li2	0.519	0.000	0.250	0.524	0.000	0.250
Li3	0.484	0.484	0.484	0.483	0.483	0.483
H1	0.195	0.306	0.393	0.175	0.310	0.397
H2	0.118	0.415	0.321	0.115	0.405	0.339
H3	0.003	0.118	0.147	0.012	0.119	0.146
H4	0.180	0.180	0.180	0.172	0.172	0.172
			Domain 2, Ref. 11			
N	0.117	0.361	0.402	0.115	0.359	0.405
B	0.113	0.113	0.113	0.114	0.114	0.114
Li1	0.281	0.000	0.250	0.286	0.000	0.250
Li2	0.519	0.000	0.250	0.523	0.000	0.250
Li3	0.484	0.484	0.484	0.484	0.484	0.484
H1	0.195	0.305	0.394	0.176	0.310	0.399
H2	0.118	0.415	0.321	0.114	0.402	0.338
H3	0.003	0.117	0.148	0.015	0.116	0.149
H4	0.180	0.180	0.180	0.174	0.174	0.174
			Ref. 12			
N	−0.152	0.112	0.367	−0.156	0.110	0.367
B	0.137	0.137	0.137	0.135	0.135	0.135
Li1	0.250	−0.030	0.000	0.250	−0.043	0.000
Li2	−0.268	0.000	0.250	−0.262	0.000	0.250
Li3	0.266	0.266	0.266	0.272	0.272	0.272
H1	0.071	0.071	0.071	0.072	0.072	0.072
H2	0.103	0.133	0.247	0.097	0.136	0.248
H3	−0.143	0.055	0.445	−0.153	0.053	0.439
H4	−0.071	0.165	0.368	−0.077	0.167	0.377

study[11] found anomalously short N-H bond lengths of 0.83–0.86 Å, while neutron scattering[12] gave lengths of 0.98–1.04 Å.

The external cell parameters obtained upon relaxing each of the three $Li_4BN_3H_{10}$ experimental structures (as well as the structures of the other phases used in our subsequent discussion of reaction thermodynamics) are summarized in Table I. The resulting structures are bcc and share the same lattice constant, $a=10.60$ Å, in good agreement with both diffraction studies.

For each of the three relaxed structures, Table II compares the calculated internal atomic coordinates with the corresponding experimental values. We note first that the average absolute deviation (δ) between theory and experiment is smallest for the neutron structure,[12] $\delta=3.6\times10^{-3}$, whereas for the x-ray structure[11] $\delta=4.4\times10^{-3}$ and $\delta=4.2\times10^{-3}$ for domains 1 and 2, respectively. The largest discrepancy between theory and experiment is in the positions of the N-bonded hydrogen atoms, H1 and H2, in the x-ray structure. (Note that the labeling convention for hydrogens is different in the neutron structure: there H1 and H2 refer to B-bonded hydrogens.) Second, while there appear to be large differences in the internal coordinates measured by Refs. 11 and 12 (Table II), after relaxation these three structures may be mapped onto one another via a series of rigid body rotations and translations. We conclude that all three experimental structures relax to essentially the same structure.

A comparison of calculated bond lengths, bond angles, and intermolecular distances is given in Table III. Overall, the relaxed structures agree best with the *intramolecular* lengths (i.e., within an NH_2 or BH_4 fragment) determined using neutron diffraction; conversely, the *intermolecular* distances from x-ray diffraction are closest to those in the relaxed theoretical structures. As for the intramolecular structure, as noted above, the major discrepancy between the experimental structures lies in the two N-H bond lengths,

TABLE III. Comparison of calculated atomic distances and angles with values determined from single-crystal x-ray diffraction (Ref. 11) and synchrotron x-ray and neutron powder diffraction (Ref. 12). Lengths (d) are given in Å, angles ($\measuredangle$) are in degrees.

	Ref. 11, domain 1		Ref. 11, domain 2		Ref. 12	
Parameter	Calculated	Experiment	Calculated	Experiment	Calculated	Experiment
			Intramolecular values			
d(N-H) (i)	1.027	0.83(2)	1.027	0.84(2)	1.027	0.983
d(N-H) (ii)	1.027	0.859	1.026	0.852	1.027	1.042
d(B-H) (i)	1.223	1.08(3)	1.225	1.11(3)	1.224	1.169
d(B-H) (ii)×3	1.225	1.137	1.225	1.121	1.223	1.270
$\measuredangle$(H-N-H)	103.5	106.2	103.5	105.9	103.5	104.9
$\measuredangle$(H-B-H)×3 (i)	108.0	108.9	107.9	109.2	107.9	107.6
$\measuredangle$(H-B-H)×3 (ii)	110.9	110.1	111.0	109.8	111.0	111.3
			Intermolecular values			
d(N-Li) (i)	2.071	2.069	2.069	2.068	2.070	2.033
d(N-Li) (ii)	2.116	2.115	2.111	2.113	2.110	2.053
d(N-Li) (iii)	2.138	2.117	2.138	2.119	2.142	2.094
d(N-Li)(iv)	2.164	2.157	2.164	2.157	2.169	2.209
d(B-Li) (i)	2.371	2.410	2.375	2.406	2.368	2.527
d(B-Li) (ii)×3	2.595	2.651	2.592	2.642	2.589	2.681

d(N-H), in the NH_2 fragment. The calculated length of 1.027 Å is in better agreement with the longer bond lengths predicted by neutron diffraction of 0.983 and 1.042 Å. Similarly, the x-ray data also underestimates B-H bond lengths in the BH_4 units relative to our DFT calculations and neutron data. Calculated bond angles agree best with those from the neutron structure.

IV. REACTION ENERGETICS

In order to examine the finite-temperature thermodynamics of reactions involving $Li_4BN_3H_{10}$, it was first necessary to calculate the ground-state structures of the phases that participate in those reactions. A summary of the compounds used, their crystal structures, and a comparison of the calculated structures to experimental data is presented in Table I. In general the agreement between experiment and theory is very good.

Some of the compounds listed in Table I are known to have several polymorphs. For example, at least three polymorphs have been reported for Li_3BN_2,[37,38,41,42] including low-temperature tetragonal (α),[37] high-temperature monoclinic (β),[38] and high-pressure body-centered tetragonal (bct) phases.[39,41,42] All three of these phases have been observed as dehydrogenation products for $Li_4BN_3H_{10}$,[4,8] and we have performed calculations on each phase to determine its relative stability as a function of temperature. The β-Li_3BN_2 phase was found to have the lowest 0 K static energy, ≈2 kJ/(mol f.u.) lower than that of either the bct or α phase. The latter two phases are degenerate in energy to within 0.1 kJ/(mol f.u.). Our 0 K energetics and structures agree well with recentcalculations reported by Pinkerton and Herbst.[39]

Vibrational contributions to the energies of each Li_3BN_2 polymorph were evaluated within the harmonic approximation. For α-Li_3BN_2 a careful evaluation of the vibrational spectra yielded doubly degenerate imaginary modes at $81i$ cm^{-1}, indicating that this phase is unstable at low temperatures. A search for alternative low-energy α-Li_3BN_2 structures was performed using molecular dynamics (MD) on an enlarged $(2\times2\times2)$ α-Li_3BN_2 supercell at $T=423$ K for 10 ps. At 1 ps intervals the current MD configuration was stored, relaxed, and the symmetry of the resulting optimized structure was determined. Four unique crystal structures were identified, with space groups (numbers): $P2_12_12_1$ (19), *Pccn* (56), *Pmmn* (59), and *Pnma* (62). These structures were then relaxed within their symmetry constraints, and were found to have energies ~1 kJ/(mol f.u.) lower than the original α-Li_3BN_2 structure [which is still 1 kJ/(mol f.u.) higher in energy than β-Li_3BN_2]. In light of these results we suggest that the crystal structure of α-Li_3BN_2 be experimentally re-assessed, and we exclude this phase from our evaluation of $Li_4BN_3H_{10}$ dehydrogenation reactions. Further information regarding our proposed structure of α-Li_3BN_2 can be found elsewhere.[43]

Unlike α-Li_3BN_2, no imaginary modes were observed in the vibrational spectra of β or bct Li_3BN_2. Using Eqs. (1) and (2), Fig. 1 plots the Gibbs free energies [Eq. (4)] of these phases as a function of temperature. Due to their similar vibrational contributions (Table IV), the free energies of the β and bct phases exhibit nearly identical temperature dependence. Consequently, the small ~2 kJ/(mol f.u.) difference in static energies noted above is sufficient to favor the monoclinic β phase as the ground state structure, and the bct-β energy difference remains roughly constant for $T<1000$ K. Based on the vibrational instability observed in α-Li_3BN_2, and the higher free energy of bct Li_3BN_2 (relative to

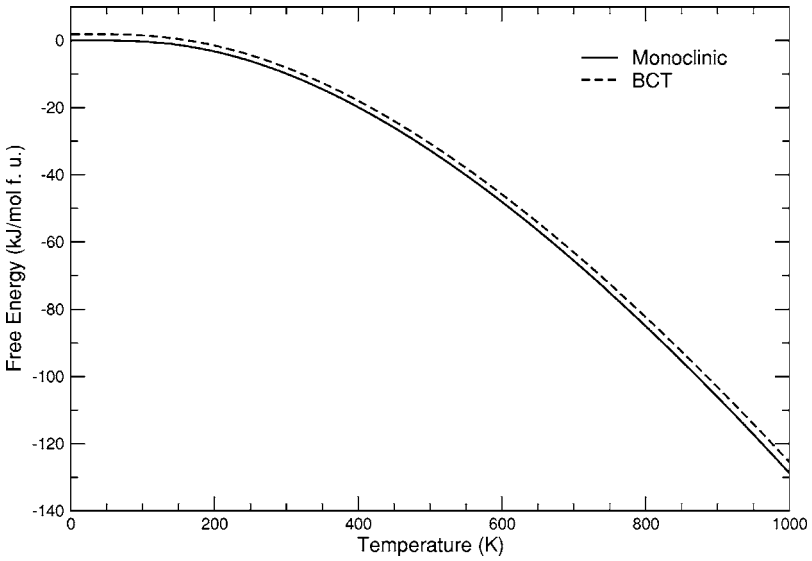

FIG. 1. Calculated Gibbs free energies [in kJ/(mol f.u.)] of monoclinic (β) and body-centered tetragonal (bct) Li_3BN_2 as a function of temperature. The energy zero is set to the static 0 K energy of β-Li_3BN_2.

β-Li_3BN_2), our subsequent thermodynamic analyses are performed assuming Li_3BN_2 resides in the low-energy β structure.

The zero-point, enthalpic, and entropic contributions to the free energy of the various phases are summarized in Table IV. As a further test of our computational methodology, there we also compare our calculated ZPE to other values reported in the literature, and find good agreement. With the exception of Li, vibrational effects are found to contribute substantially to the free energies of these systems. For example, in $Li_4BN_3H_{10}$ the ZPE exceeds 300 kJ/mol.

A comparison of formation energies for the compounds used in this study (relative to the elements in their standard states) is presented in Table V. Three reports[39,45,26] based on DFT calculations have also recently evaluated formation energies for some of these compounds, and the present calculations are in good agreement with their findings. Furthermore, the agreement with experimental enthalpies is reasonable (generally on the order of 10%), which is representative of the accuracy obtained via density functional methods for reactions involving molecular species.[50] As expected, the largest percentage discrepancy is for the ammonia molecule.[51] Two general trends in the data are evident: (i) With the exception of ammonia, the DFT enthalpies ($\Delta H^{T=300\ \mathrm{K}}$) are more positive than the experimental values, and (ii) the inclusion of dynamical contributions ($\Delta E \rightarrow \Delta H^{T=300\ \mathrm{K}}$) results in more positive formation energies.

TABLE IV. Calculated vibrational contributions (at $T=300$ K) to the free energies of phases used in this study. ZPE refers to the zero-point energy, given by $H_{\mathrm{vib}}(T=0)$ [Eq. (1)]; $E_{\mathrm{vib}}=H_{\mathrm{vib}}-\mathrm{ZPE}$ (omitting the k_BT molecular terms); S_{vib} is the vibrational entropy, Eq. (2). Units are kJ mol^{-1} for ZPE and E_{vib}, and J mol^{-1} K^{-1} for S_{vib}.

System	ZPE	ZPE other	Reference	$E_{\mathrm{vib}}^{T=300\ \mathrm{K}}$	$S_{\mathrm{vib}}^{T=300\ \mathrm{K}}$
H_2	25.7	25.7, 26.1, 26.3	44 and 45 26	≈ 0	≈ 0
N_2	14.0	14.4	26	≈ 0	≈ 0
NH_3	87.8	89.7	46	0.1	0.4
Li	3.9	3.9	45	4.3	27.7
B	12.5	12.2	45	1.1	5.3
BN	29.9	30.9	47		
LiH	21.7	21.4, 21.8	45 and 35	3.5	17.7
Li_3N	28.0	28.6	33		
$LiNH_2$	69.0	69.1, 69.5, 69.8	33 and 35 26	8.9	51.6
Li_2NH	46.7	46.7, 47.1	26 and 35	9.6	52.9
$LiBH_4$	107.1	103.0, 106.5, 108.1	45 and 44 48	10.8	63.6
Li_3BN_2	52.2			15.3	83.8
$Li_4BN_3H_{10}$	314.4			37.0	213.4

TABLE V. Comparison of calculated formation energies [with respect to the elements, in kJ/(mol f.u.)] with existing experimental and theoretical data. ΔE refers to differences in static 0 K energies; formation enthalpies (ΔH) and free energies (ΔG) are based on Eqs. (3) and (4), respectively. Experimental data are from Refs. 28 and 49; theoretical data are from a set of recent DFT calculations (Refs. 9, 45, and 26).

System	ΔE	Reference	$\Delta H^{T=300\ \mathrm{K}}$	Reference	$\Delta G^{T=300\ \mathrm{K}}$	Reference
NH_3	−98.0		−63.2		−33.6	
			−45.9	28	−16.2	28
BN	−233.8		−227.4		−198.9	
			−250.9	28	−224.9	28
LiH	−83.6		−83.8		−61.2	
	−81	45	−90.6	28	−68.3	28
	−83.9	26	−84.6	26		
Li_3N	−148.7		−145.9		−109.8	
			−164.6	28	−128.4	28
$LiNH_2$	−196.6		−172.6		−111.7	
	−196.5	26	−176	49		
			−173.1	26		
Li_2NH	−196.0		−184.5		−135.3	
	−194.0	26	−222	49		
			−184.1	26		
$LiBH_4$	−205.9		−178.6		−109.2	
	−194	45	−190.5	28	−124.3	28
Li_3BN_2	−497.4		−490.6		−433.6	
	−497	39				

Using the energetic contributions from Table IV, in Table VI we evaluate the thermodynamics for two $Li_4BN_3H_{10}$ formation reactions. Reaction (a) considers formation from the elemental phases in their standard states, and reaction (b) corresponds to the synthesis route employed in the literature[4,7,12] involving a mixture of $LiNH_2$ and $LiBH_4$. (We consider only the stoichiometric[12] 3:1 ratio of $LiNH_2$ to $LiBH_4$.[52]) The energetics of each reaction are decomposed into a sequence having increasingly more physical contributions to the reaction thermodynamics, $\Delta E \rightarrow \Delta H^{T=0\ \mathrm{K}} \rightarrow \Delta H^{T=300\ \mathrm{K}} \rightarrow \Delta G^{T=300\ \mathrm{K}}$, which allows us to gauge the importance of these contributions in comparison to the common practice of evaluating only static 0 K energetics. (ΔE refers to differences in the static 0 K energies [E in Eq. (3)], and $\Delta H^{T=0\ \mathrm{K}}$ adds ZPE contributions to ΔE.) Both formation reactions in Table VI are predicted to be exothermic ($\Delta H < 0$), in agreement with reports of spontaneous $Li_4BN_3H_{10}$ formation from the literature.[4,7,12] As expected, formation from the elements vs from the hydride mixture is a substantially more exothermic process.

It is noteworthy that dynamical contributions to the reaction energies are significant in reaction (a) ($\Delta E \neq \Delta H$), but appear to play a minor role in reaction (b) ($\Delta E \approx \Delta H$). By examining the values presented in Table IV for the phases participating in reaction (b) ($Li_4BN_3H_{10}$, $LiNH_2$, and $LiBH_4$) we see that these terms are sizable, but that they largely cancel out. This cancellation effect can be understood by the similarities in internal bonding shared by these three phases: $Li_4BN_3H_{10}$, with its Li^+, BH_4^-, and NH_2^- ions is essentially an amalgam of the structures present in $LiNH_2$ and $LiBH_4$.

Turning now to the dehydrogenation of $Li_4BN_3H_{10}$, we note first that although several dehydrogenation products have been observed in experimental studies,[4,5,7,8] the precise identity and respective proportions of these phases have not yet been definitively determined.[4,7] For example, Aoki *et al.* reported unidentified diffraction peaks after dehydrogenation at $2\theta = 25$ and 35 degrees. A technique for predicting possible decomposition pathways would be of significant value in helping to understand these reactions. However, decomposition pathways and products are difficult to predict *a priori*.

TABLE VI. Formation energies of $Li_4BN_3H_{10}$ [in kJ/(mol $Li_4BN_3H_{10}$)]. ΔE corresponds to the static 0 K DFT energies; $\Delta H^{T=0\ \mathrm{K}}$ adds the zero-point energies to ΔE; $\Delta H^{T=300\ \mathrm{K}}$ [Eq. (3)] adds finite-temperature vibrational (and molecular rotational+translational+pV) energies to $\Delta H^{T=0\ \mathrm{K}}$; $\Delta G^{T=300\ \mathrm{K}}$ [Eq. (4)] includes all of the contributions to $\Delta H^{T=300\ \mathrm{K}}$ and adds vibrational (solids) or tabulated (molecular) entropies.

Reaction no.	Reaction	ΔE	$\Delta H^{T=0\ \mathrm{K}}$	$\Delta H^{T=300\ \mathrm{K}}$	$\Delta G^{T=300\ \mathrm{K}}$
(a)	$4\ \mathrm{Li}+\mathrm{B}+\frac{3}{2}\mathrm{N_2}+5\mathrm{H_2} \rightarrow \mathrm{Li_4BN_3H_{10}}$	−806.9	−670.2	−708.1	−454.6
(b)	$3\ \mathrm{LiNH_2}+\mathrm{LiBH_4} \rightarrow \mathrm{Li_4BN_3H_{10}}$	−11.3	−11.2	−11.8	−10.2

TABLE VII. Calculated reaction energies [ΔE in kJ/(mol H_2)], enthalpies [ΔH in kJ/(mol H_2)], and free energies [ΔG in kJ/(mol products)] for candidate $Li_4BN_3H_{10}$ dehydrogenation reactions.

Reaction no.	Reaction	ΔE	$\Delta H^{T=0\ K}$	$\Delta H^{T=300\ K}$	$\Delta H^{T=460\ K}$	$\Delta G^{T=300\ K}$	$\Delta G^{T=460\ K}$
(c)	$Li_4BN_3H_{10} \rightarrow Li_3BN_2 + LiNH_2 + 4H_2$	28.2	5.7	11.2	12.5	−88.8	−161.3
(d)	$Li_4BN_3H_{10} \rightarrow Li_3BN_2 + \frac{1}{2}Li_2NH + \frac{1}{2}NH_3 + 4H_2$	40.6	17.7	23.4	24.3	−61.4	−145.2
(e)	$Li_4BN_3H_{10} \rightarrow Li_3BN_2 + LiH + NH_3 + 3H_2$	42.6	17.5	23.5	24.0	−71.6	−148.0
(f)	$Li_4BN_3H_{10} \rightarrow Li_3BN_2 + LiH + \frac{1}{2}N_2 + \frac{9}{2}H_2$	50.2	24.1	29.7	30.8	−38.2	−131.0
(g)	$Li_4BN_3H_{10} \rightarrow Li_3BN_2 + Li + \frac{1}{2}N_2 + 5H_2$	61.9	37.4	43.5	44.6	23.0	−82.2
(h)	$Li_4BN_3H_{10} \rightarrow Li_3BN_2 + Li + NH_3 + \frac{7}{2}H_2$	60.4	37.5	44.1	44.7	−10.5	−99.2
(i)	$Li_4BN_3H_{10} \rightarrow 2LiNH_2 + 2LiH + BN + 2H_2$	6.4	−19.4	−16.1	−15.4	−90.1	−121.2
(j)	$Li_4BN_3H_{10} \rightarrow LiNH_2 + Li_3N + BN + 4H_2$	56.9	35.8	40.5	41.3	34.1	−34.9
(k)	$Li_4BN_3H_{10} \rightarrow 4LiH + BN + N_2 + 3H_2$	79.6	44.1	48.5	48.8	11.1	−60.7
(l)	$Li_4BN_3H_{10} \rightarrow 2Li_2NH + BN + 4H_2$	45.3	23.3	27.9	28.8	−14.9	−83.3
(m)	$Li_4BN_3H_{10} \rightarrow 2LiNH_2 + BN + 2Li + 3H_2$	60.0	39.5	45.1	46.2	32.3	−23.6
(n)	$Li_4BN_3H_{10} \rightarrow LiNH_2 + Li_2NH + LiH + BN + 3H_2$	32.3	9.1	13.2	14.1	−52.5	−102.3
(o)	$Li_4BN_3H_{10} \rightarrow Li_2NH + 2LiH + BN + NH_3 + 2H_2$	55.9	28.5	32.7	32.1	−35.4	−88.9
(p)	$Li_4BN_3H_{10} \rightarrow LiNH_2 + 3LiH + BN + NH_3 + H_2$	27.7	−9.1	−6.6	−8.8	−73.0	−107.9
(q)	$Li_4BN_3H_{10} \rightarrow Li_3N + LiH + BN + NH_3 + 3H_2$	80.9	57.7	62.6	62.4	51.3	−21.6
(r)	$Li_4BN_3H_{10} \rightarrow \frac{1}{2}Li_2NH + Li_3N + BN + \frac{1}{2}NH_3 + 4H_2$	69.3	47.8	52.7	53.2	61.5	−18.8
(s)	$Li_4BN_3H_{10} \rightarrow Li_3BN_2 + \frac{1}{3}Li_3N + \frac{2}{3}NH_3 + 4H_2$	48.7	26.0	31.7	32.5	−35.9	−123.6

To this end, we have scanned through the thermodynamics of a large number of candidate dehydrogenation reactions over a wide temperature range in order to identify the energetically favored products.[52]

Calculated thermodynamics for 17 candidate $Li_4BN_3H_{10}$ dehydrogenation reactions are listed in Table VII. In addition to the room-temperature energetics, there we also present data for $T=460$ K, which is slightly below the melting point of pure $Li_4BN_3H_{10}$. Unlike the $Li_4BN_3H_{10}$ formation reaction, which can proceed at room temperature,[4] dehydrogenation of $Li_4BN_3H_{10}$ has been reported only at elevated temperatures. In the case of pure $Li_4BN_3H_{10}$, dehydrogenation occurs above ~520 K, about 60 degrees above the melting temperature.[4] However, a significant reduction in dehydrogenation temperature was observed upon the addition of a small amount of a Pt/Vulcan carbon catalyst.[6] In this latter case hydrogen release occurred from the solid phase at $T > 390$ K. To more completely assess the dehydrogenation thermodynamics over a range of relevant temperatures, in Fig. 2 we plot the enthalpies and free energies of the candidate reactions for $T=0-1000$ K.

Out of the 17 reactions considered, three reactions—(i), (c), and (f)—emerge as the most favorable reactions in distinct temperature regimes (see Fig. 2, bottom panel). For low temperatures reaction (i) is preferred, followed at increasing temperatures by reaction (c) and reaction (f). More specifically, the favored products and their respective temperature ranges of stability are

$$2LiNH_2 + 2LiH + BN + 2H_2 \quad (0 \le T \le 300\ K),$$

$$Li_3BN_2 + LiNH_2 + 4H_2 \quad (300 \le T \le 700\ K),$$

$$Li_3BN_2 + LiH + \frac{1}{2}N_2 + \frac{9}{2}H_2 \quad (700\ K \le T).$$

The relatively large entropy of the gas-phase products plays an important role in determining which reaction is favored at a given temperature. Reactions yielding greater quantities of gaseous products should be favored with increasing T, and this is consistent with the observed trend: reaction (i), 2 mols → reaction (c), 4 mols → reaction (f), 5

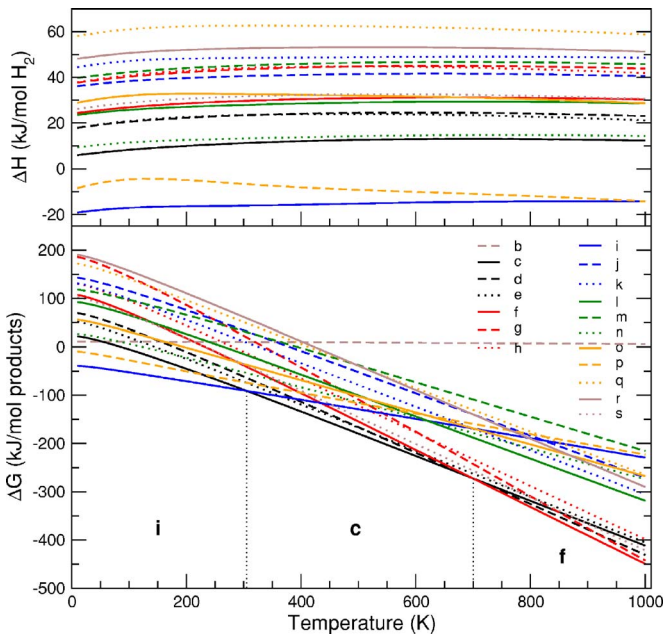

FIG. 2. (Color online) Calculated enthalpies (ΔH, top panel) and free energies (ΔG, bottom panel) of candidate $Li_4BN_3H_{10}$ dehydrogenation reactions as a function of temperature at $p=1$ bar. The reactions are labeled as in Table VII.

mols. (It should be noted that at high temperatures—and certainly above the melting point of $Li_4BN_3H_{10}$—the harmonic approximation will no longer be valid, so we expect some decrease in accuracy with increasing T.)

Of the three favorable dehydrogenation reactions, only reaction (c), $Li_4BN_3H_{10} \rightarrow Li_3BN_2 + LiNH_2 + 4H_2$, takes place within the temperature range where H_2 desorption (from undoped $Li_4BN_3H_{10}$) has been experimentally observed ($T \sim 520-630$ K). While our prediction of Li_3BN_2 as a dehydrogenation product is consistent with experimental observations, we are not aware of any reports indicating the presence of $LiNH_2$. This discrepancy is likely due to the fact that most experiments have been performed on off-stoichiometric $Li_4BN_3H_{10}$ formed from 2:1 $LiNH_2$:$LiBH_4$ mixtures. Mixtures with this composition are deficient in the Li and N presumably needed to yield the additional amide present in our calculations.

The calculated enthalpy for reaction (c) ranges from 11.2 to 12.8 kJ/(mol H_2) for $T=300-500$ K, indicating that H_2 release is a weakly endothermic process. For the higher-temperature reaction (f), dehydrogenation is likewise predicted to be endothermic with a slightly larger enthalpy of ~ 31 kJ/(mol H_2). Only the low temperature reaction (i) with $\Delta H \approx -(16-19)$ kJ/(mol H_2) is found to be exothermic. It would be interesting to test whether the predicted temperature-dependent decomposition sequence [(i)→(c)→(f)] could be observed experimentally by holding $Li_4BN_3H_{10}$ at temperatures within each of the reaction regimes for long times.

Based on the data presented in Fig. 2 and Table VII, H_2 desorption from $Li_4BN_3H_{10}$ is thermodynamically favorable at essentially all non-zero temperatures: the negative free energies of dehydrogenation suggest that $Li_4BN_3H_{10}$ is metastable with respect to decomposition via one of the reactions (i), (c), or (f). On the other hand, experiments[4] on pure $Li_4BN_3H_{10}$ indicate that desorption does not take place until the temperature is raised above 520 K. Taken together, these factors suggest that the relatively high temperatures needed in practice for H_2 release are a consequence of poor kinetics, not unfavorable thermodynamics.

An important distinction between our calculations and the experimental dehydrogenation of undoped $Li_4BN_3H_{10}$ concerns the phase of $Li_4BN_3H_{10}$ present during the dehydrogenation reaction. As mentioned above, pure $Li_4BN_3H_{10}$ releases hydrogen from the molten state.[4] Similarly, H_2 release from other hydride phases, such as $LiBH_4$, also occurs from the molten state.[53] Due to the computational expense associated with obtaining precise energetics for liquids using DFT, this study, and previous studies on $LiBH_4$,[45,53] have modeled the dehydrogenation reaction as a solid-state reaction. Since the enthalpy of the liquid phase will be more positive than that of the corresponding solid phase, the calculated solid-state enthalpy of reaction (c) evaluated at the melting point (T_{mp}), $\Delta H^{T_{mp}} = 12.5$ kJ/(mol H_2), represents an *upper bound* on the enthalpy for desorption from liquid $Li_4BN_3H_{10}$. It will be possible to more precisely estimate the magnitude by which ΔH is overestimated once the latent heat of melting for $Li_4BN_3H_{10}$ has been measured. Until such data become available, it nevertheless seems reasonable to conclude that the dehydrogenation of $Li_4BN_3H_{10}$ is either weakly endothermic or exothermic. This conclusion is consistent with the failed attempts at rehydriding $Li_4BN_3H_{10}$ reported thus far in the literature,[4] as a small (positive) enthalpy of dehydrogenation will result in a similarly small thermodynamic driving force for rehydriding. On the other hand, for $Li_4BN_3H_{10}$ doped with Pt/Vulcan carbon,[6] dehydrogenation begins below T_{mp}. In this case our approach of modeling solid state reactions more accurately captures the true phase behavior of $Li_4BN_3H_{10}$, neglecting the possible formation of C- or Pt-containing compounds.

V. CONCLUSION

Density functional theory calculations have been employed to study the crystal structure and the finite-temperature formation and dehydrogenation thermodynamics of $Li_4BN_3H_{10}$. The calculations have resolved the discrepancies in hydrogen bond lengths between the separate structures determined via x-ray and neutron diffraction experiments, and suggest that the neutron data yields a slightly more accurate description of the crystal structure. All three of the reported experimental crystal structures relax to essentially the same structure.

For reaction energetics, our calculations indicate that $Li_4BN_3H_{10}$ formation is exothermic, and that the dehydrogenation enthalpy of solid-state $Li_4BN_3H_{10}$ is temperature dependent: H_2 release is exothermic at low temperatures, and weakly endothermic at the higher temperatures probed by recent experiments. A nonzero latent heat for $Li_4BN_3H_{10}$ melting will reduce the dehydrogenation enthalpy from the liquid state (relative to the solid state), but the size of this effect is still to be determined. To help clarify the identity of the phases produced via dehydrogenation we have performed a computational search over 17 candidate dehydrogenation reactions, and identified three reactions having favorable thermodynamics spanning the temperature range $T=0-1000$ K. All three of these reactions exhibit a decrease in free energy, suggesting that $Li_4BN_3H_{10}$ is a metastable phase. For temperatures where H_2 desorption has been experimentally observed, the thermodynamically favored reaction is $Li_4BN_3H_{10} \rightarrow Li_3BN_2 + LiNH_2 + 4H_2$, with an enthalpy of 11.2–12.8 kJ/(mol H_2). The relatively small dehydriding enthalpies are consistent with the failed re-hydriding attempts reported in the literature, and suggest that hydrogen release from $Li_4BN_3H_{10}$ is a kinetically—rather than thermodynamically—hindered process.

Note added. Recently, two additional studies of $Li_4BN_3H_{10}$ were brought to our attention.[54,55] In one study Noritake and co-workers[55] performed a crystal structure analysis of $Li_4BN_3H_{10}$ using synchrotron x-ray diffraction. While they found external structural parameters (bcc, space group $I2_13$, $a=10.67$ Å) consistent with the two reports cited previously,[11,12] the reported N–H bond lengths were more

consistent with the neutron data of Ref. 12 (and with our calculated N–H distances) than the x-ray data of Ref. 11. In the other recent study, Herbst and Hector[54] examined the electronic structure and energetics of $Li_4BN_3H_{10}$ using DFT. Our results appear to be consistent with their findings.

ACKNOWLEDGMENTS

The authors thank D. Halliday, A. Sudik, and J. Yang for reviewing a preliminary version of this manuscript. V.O. thanks the U.S. Department of Energy for financial support under Grant No. DE-FG02-05ER46253.

[1] U. S. National Academy of Sciences, *The Hydrogen Economy: Opportunties, Cost, Barriers and R&D Needs* (National Academies Press, Washington, D.C., 2004).

[2] L. Schlapbach and A. Züttel, Nature (London) **414**, 353 (2001).

[3] http://www.eere.energy.gov/hydrogenandfuelcells/storage/pdfs/targets_onboard_hydro_storage.pdf

[4] F. E. Pinkerton, G. P. Meisner, M. S. Meyer, M. P. Balogh, and M. D. Kundrat, J. Phys. Chem. B **109**, 6 (2005); see also supplementary information accompanying that paper.

[5] G. P. Meisner, M. L. Scullin, M. P. Balogh, F. E. Pinkerton, and M. S. Meyer, J. Phys. Chem. B **110**, 4186 (2006).

[6] F. E. Pinkerton, M. S. Meyer, G. P. Meisner, and M. P. Balogh, J. Phys. Chem. B **110**, 7967 (2006).

[7] M. Aoki, K. Miwa, T. Noritake, G. Kitahara, Y. Nakamori, S. Orimo, and S. Towata, Appl. Phys. A: Mater. Sci. Process. **80**, 1409 (2005).

[8] Y. Nakamori, A. Ninomiya, G. Kitahara, M. Aoki, T. Noritake, K. Miwa, Y. Kojima, and S. Orimo, J. Power Sources **155**, 447 (2006).

[9] B. Bogdanović and M. Schwickardi, J. Alloys Compd. **253-254**, 1 (1997).

[10] A. Gutowska *et al.*, Angew. Chem., Int. Ed. **44**, 3578 (2005).

[11] Y. E. Filinchuk, K. Yvon, G. P. Meisner, F. E. Pinkerton, and M. P. Balogh, Inorg. Chem. **45**, 1433 (2006).

[12] P. A. Chater, W. I. F. David, S. R. Johnson, P. P. Edwards, and P. A. Anderson, Chem. Commun. (Cambridge) **23**, 2439 (2006).

[13] P. Hohenberg and W. Kohn, Phys. Rev. **136**, B864 (1964).

[14] W. Kohn and L. J. Sham, Phys. Rev. **140**, A1133 (1965).

[15] J. P. Perdew *et al.*, Phys. Rev. B **46**, 6671 (1992).

[16] G. Kresse and J. Furthmüller, Phys. Rev. B **54**, 11169 (1996).

[17] P. E. Blöchl, Phys. Rev. B **50**, 17953 (1994).

[18] G. Kresse and D. Joubert, Phys. Rev. B **59**, 1758 (1999).

[19] H. J. Monkhorst and J. D. Pack, Phys. Rev. B **13**, 5188 (1976).

[20] More specifically, the potentials employed for evaluating 0 K energies and geometries were (in the parlance of the VASP database) Li_sv, B_h, N_h, and H_h, with respective valence electron configurations of $1s^2\,2s^1$, $2s^2\,2p^1$, $2s^2\,2p^3$, and $1s^1$.

[21] D. C. Wallace, *Thermodynamics of Crystals* (John Wiley & Sons, New York, 1972).

[22] J. M. Rickman and R. LeSar, Annu. Rev. Mater. Res. **32**, 195 (2002).

[23] S. Wei and M. Y. Chou, Phys. Rev. Lett. **69**, 2799 (1992).

[24] The geometry of each structure was reoptimized using the softer PAW set before the dynamical matrix calculations were performed.

[25] Our somewhat nonstandard approach of using softer potentials to determine the vibrational spectra of the solid phases, but hard (semicore) potentials for the remaining properties (0 K energetics, ground-state geometries, and molecular vibrational spectra) is based on three considerations: First, the softer PAW set allows for more efficient calculations with a reduced plane-wave cutoff energy, thus permitting larger supercells and, consequently, smaller finite-size effects in the phonon spectrum. Second, our calculated formation energies for LiH, $LiNH_2$, and Li_2NH at $T=300$ K agree with the hard PAW results in Ref. 26 to within 1 kJ/(mol f.u.). Third, testing revealed that the hard potentials yielded molecular vibrational frequencies that were in slightly better agreement with experimental data than those obtained with the softer PAW set. For example, for N_2, where the differences between calculated vibrational frequencies are largest, we find 2338 (2452) cm^{-1} from the hard (soft) PAW sets, compared with an experimental value of 2359 cm^{-1} (Ref. 27). However, this slight discrepancy in frequencies has only a small impact on vibrational thermodynamic properties—for example, ZPEs calculated with both PAW sets differ by 0.7 kJ/(mol f.u.) at most. It therefore seems likely that an approach where *all* vibrational properties (solids and molecules) were evaluated using the softer potentials would also yield reasonably precise results. We thus conclude that our approach of mixing potentials gives results comparable in precision to those obtained with the hard PAW set alone, but without the associated computational expense.

[26] J. F. Herbst and L. G. Hector, Jr., Phys. Rev. B **72**, 125120 (2005).

[27] *CRC Handbook of Chemistry and Physics*, edited by D. R. Lide, 86th ed. (Taylor and Francis, London, 2005).

[28] M. W. Chase, Jr., *NIST-JANAF Thermochemical Tables*, 4th ed. (American Chemical Society, Washington, DC, 1998).

[29] A. C. Switendick and B. Morosin, in *Boron-Rich Solids*, edited by D. Emin, T. L. Aselage, A. C. Switendick, B. Morosin, and C. L. Beckel, AIP Conf. Proc. No. 231 (AIP, New York, 1991), p. 205.

[30] R. H. Wentorf, Jr., J. Chem. Phys. **26**, 956 (1957).

[31] *Pearson's Handbook of Crystallographic Data for Intermetallic Phases*, edited by P. Villars and L. D. Calvert, 2nd ed. (ASM International, Materials Park, OH, 1991), Vols. 2,4.

[32] J. P. Vidal and G. Vidal-Valat, Acta Crystallogr., Sect. B: Struct. Sci. **42**, 131 (1986).

[33] K. Miwa, N. Ohba, S. I. Towata, Y. Nakamori, and S. I. Orimo, Phys. Rev. B **71**, 195109 (2005).

[34] H. Jacobs and R. Juza, Z. Anorg. Allg. Chem. **391**, 271 (1972).

[35] B. Magyari-Köpe, V. Ozoliņš, and C. Wolverton, Phys. Rev. B **73**, 220101(R) (2006).

[36] K. Cenzual, L. M. Gelato, M. Penzo, and E. Parthe, Acta Crystallogr., Sect. B: Struct. Sci. **47**, 433 (1991).

[37] H. Yamane, S. Kikkawa, and M. Koizumi, J. Solid State Chem. **71**, 1 (1987).

[38] H. Yamane, S. Kikkawa, H. Horiuchi, and M. Koizumi, J. Solid State Chem. **65**, 6 (1986).

[39] F. E. Pinkerton and J. F. Herbst, J. Appl. Phys. **99**, 113523 (2006).

[40] J.-P. Soulie, G. Renaudin, R. Cerny, and K. Yvon, J. Alloys

Compd. **346**, 200 (2002).
[41] R. H. Wentorf, Jr., J. Phys. Chem. **34**, 809 (1961).
[42] R. C. DeVries and J. F. Fleischer, Mater. Res. Bull. **4**, 433 (1969).
[43] D. J. Siegel (unpublished).
[44] T. J. Frankcombe and G.-J. Kroes, Phys. Rev. B **73**, 174302 (2006).
[45] K. Miwa, N. Ohba, S. I. Towata, Y. Nakimori, and S. I. Orimo, Phys. Rev. B **69**, 245120 (2004).
[46] J. E. Northrup, R. Di Felice, and J. Neugebauer, Phys. Rev. B **56**, R4325 (1997).
[47] G. Kern, G. Kresse, and J. Hafner, Phys. Rev. B **59**, 8551 (1999).
[48] Z. Łodziana and T. Vegge, Phys. Rev. Lett. **93**, 145501 (2004).
[49] P. Chen, Z. Xiong, J. Luo, J. Lin, and K. L. Tan, Nature (London) **420**, 302 (2002).
[50] L. A. Curtiss, K. Raghavachari, P. C. Redfern, and J. A. Pople, J. Chem. Phys. **106**, 1063 (1997).
[51] The discrepancy in calculated vs experimental enthalpy for Li_2NH has been noted in Ref. 26, and it has been suggested that the experimental measurement be revisited in light of the good agreement for the other Li-containing compounds: LiH, $LiNH_2$, and $LiBH_4$. To our knowledge the formation enthalpy of Li_2NH reported in Ref. 49 has not been independently confirmed.
[52] Due to the computational difficulty associated with treating a nonstoichiometric phase, our calculations are restricted to the stoichiometric composition "$Li_4BN_3H_{10}$," whereas most experiments have focused on 2:1 $LiNH_2$:$LiBH_4$ off-stoichiometric "$Li_3BN_2H_8$" mixtures, which have been found to minimize NH_3 release (Ref. 5).
[53] T. J. Frankcombe, G.-J. Kroes, and A. Züttel, Chem. Phys. Lett. **405**, 73 (2005).
[54] J. F. Herbst and L. G. Hector, Jr., Appl. Phys. Lett. **88**, 231904 (2006).
[55] T. Noritake, M. Aoki, S. Towata, A. Ninomiya, Y. Nakamori, and S. Orimo, Appl. Phys. A: Mater. Sci. Process. **83**, 277 (2006).